Magnetization of ultrathin bcc Fe films on MgO

Y. Y. Huang, C. Liu, and G. P. Felcher
Material Science Division, Argonne National Laboratory, Argonne, Illinois 60439
(Received 6 March 1992)

The magnetization of body-centered-cubic iron was measured by means of polarized neutron reflection on a set of films of different thickness (4, 6, 8, and 16 Å). The films were epitaxially deposited onto polished (100) MgO substrates and covered by protective layers of gold. The results show that at 40 K all films are ferromagnetic, with an average magnetic moment per iron equal to $2.2\pm0.2\mu_B$ regardless of film thickness. However, the thinnest films exhibit a Curie temperature lower than that of the bulk and a magnetization axis tilted out of the film surface. These results are discussed in the light of the detailed morphology of the films, and compared with the theoretical predictions.

INTRODUCTION

One of the major themes of the research on magnetism during the last decades has been the understanding of the effect of reduced dimensionality at the surface of solids or in very thin layers. Early theoretical studies[1] already showed that at the surface of metals the magnetic moments per atom are intermediate between the value in the solid and those (usually higher) of the free atoms. On the other hand, two-dimensional layers could not even order magnetically[2] if the magnetic interaction was not sufficiently anisotropic. In more recent years, numerous *a priori* calculations have shown that monolayers of 3*d* transition metals remain ferromagnetic when free standing or deposited on various substrates.[3–7] However, the magnetic moment is predicted to undergo a profound alteration when the thickness of the film approaches monolayer limit. For example, Li and Freeman have recently calculated the equilibrium properties of a free-standing iron monolayer, and found that the Fe moment ($3.1\mu_B$) is remarkably enhanced[8] compared to the bulk value ($2.2\mu_B$). Similar enhancement ($3.07\mu_B$) was obtained in calculations in which a monolayer of iron was set on a substrate of gold or of magnesium oxide.[9,10] The virtual identity of the results with the free monolayer has been attributed to the fact that no electronic transfer occurs with the substrates, that also crystallizes with cell spacings not very different from those of iron. For thicker iron layers, the magnetic moments at the surface remain enhanced, while the atoms embedded in the layer have moments close to the bulk. In short, a system like Fe/MgO should resemble rather well an ideal two-dimensional system, and at the same time adequate samples can be prepared for experimental work.

Numerous experimental studies have been done recently on ultrathin films of iron. These have been epitaxially deposited on single-crystal substrates of Cu,[11,12] Ag,[13–15] Au,[16] Pd,[17] W,[18] and MgO (Ref. 19) and studied by spin-polarized photoemission, Kerr effect, conversion electrons, Mössbauer spectroscopy, and spin-polarized low-energy electron diffraction (LEED). These studies have demonstrated the presence of ferromagnetic ordering and perpendicular surface anisotropy in monolayer thick iron films. However, the determination of the absolute magnetic moment per atom of an ultrathin film is still a tremendous challenge for experimentalists.

One of the most promising techniques is polarized neutron reflection (PNR). Experiments were proposed[20] and later successfully implemented to determine the magnetic moments in Fe and Co films[21] as thin as 10 Å. Being an optical technique, PNR is much more selective in viewing magnetization than SQUID magnetometry. To start with, the location of the magnetic signal in the sample is identified, and thus the magnetic response of the substrate and overlayer does not need to be subtracted. In the same breath, the optical signal assures that iron has been laid down largely as a film, and not (for instance) as an assembly of droplets having equivalent thickness. In this paper we present results of a series of PNR studies on a set of bcc iron on MgO (100).

SAMPLE PREPARATION

All samples were prepared in 10^{-11} Torr ultrahigh vacuum and characterized by low-energy electron diffraction and Auger spectroscopy. Epitaxially polished MgO (100) single crystals were used as substrates. MgO exhibited a $p(1\times1)$ LEED pattern characteristic of the bulk terminated structure even before any cleaning treatment in vacuum. Carbon and/or CO impurities on the surface, as detected by monolayer level carbon Auger signals, were removed by 500-eV Ar^+ sputtering for 5 min at a grazing angle of about 30°. The Fe films were grown at room temperature from a resistive evaporator about 3 in. away from the substrate with the Fe beam normal to the substrate surface. LEED observations confirmed that Fe grows epitaxially on MgO (100). Under such conditions, it has been reported in literature[22] that Fe films less than 10 Å thick have a body-centered-tetragonal structure, and a body-centered-cubic structure develops with increasing thickness.

Separate measurements of the Auger intensity versus deposition time were carried out beforehand to study the growth mode of Fe on MgO (100). As shown in Fig. 1, the data fit quite well to exponential growth and decay curves without distinct break points, an indication of a

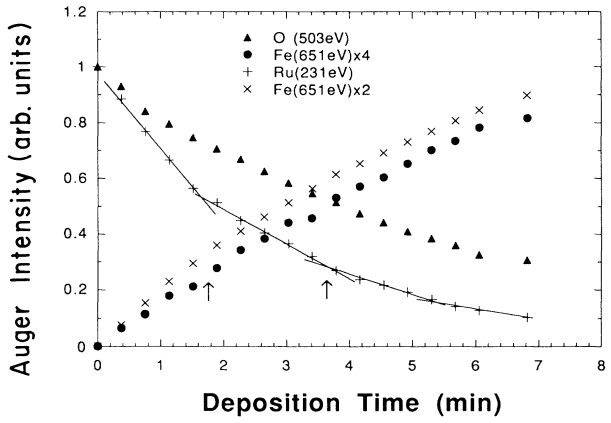

FIG. 1. Auger intensity vs deposition-time measurements for iron grown on Ru (0001) (cross) and on MgO (100) (solid circles) at room temperature. The two sets of iron data are normalized to that of Ru and oxygen, respectively. Fe signals are multiplied by 4 (for Fe/MgO) and by 2 (for Fe/Ru), respectively. The arrows indicate the completion of the first and second monolayers of Fe on Ru.

simultaneous-multilayer growth mode.[23] In this mode, film grows with a series of terraces of different heights and multilayers are built up simultaneously with the growth of the first layer. Similar observations were reported by Urano and Kanji,[19] but were interpreted as layer-by-layer growth.

To calibrate the evaporation rate, the Auger measurements were repeated for Fe/Ru (0001), which is known to have a layer-by-layer growth.[24,25] Repeated Auger measurements confirmed that the evaporation rate remained constant within 5% during the time period of the experiments. The deposition time needed to complete one monolayer of Fe on Ru (0001) was then used to determine the thickness of Fe/MgO (100). Both oxygen and ruthenium Auger signals are presented in Fig. 1. The two signals appear different because the Auger electrons emitted by ruthenium ($E=231$ eV) are considerably less energetic than those emitted by oxygen ($E=503$ eV). Once scaled for the different penetration depths, the two signals approach each other indicating that even for Fe/MgO the growth is not too different from the layer-by-layer mode.

Four $0.04\times1\times1$ in. MgO (100) were mounted on four separate sample holders which were attached to a common manipulator so that each MgO (100) could be rotated for individual Ar^+ sputtering, Fe depositing, and Au coating. Four samples with average Fe layer thicknesses of about 4, 6, 8, and 16 Å were sequentially made. For simplicity, we will refer to each sample by its nominal thickness. A better than 90% uniformity was confirmed by measuring Auger signals at different positions along the samples. An estimated 200 Å Au film was added on each Fe/MgO (100) from a resistive evaporator at a grazing angle of about 45°. The average Au thickness was obtained from a quartz crystal thickness monitor facing the Au evaporator. A wedge-shaped Au layer was expected based on geometry consideration.

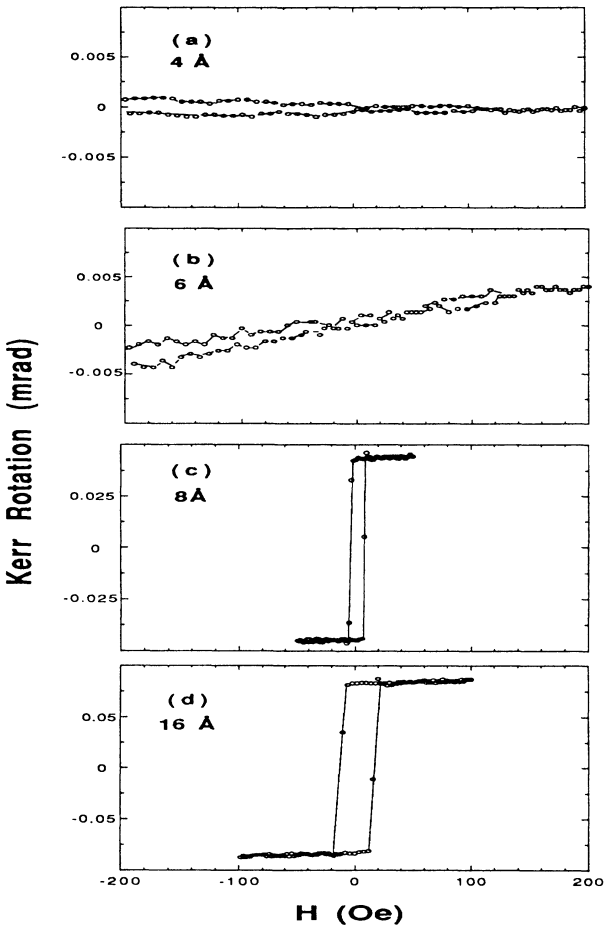

FIG. 2. Rotation of the polarization vector of light reflected by iron films of different thickness, deposited on MgO (100). The surface magneto-optical Kerr-effect measurements were done at room temperature, with a cycling magnetic field applied parallel to the surface.

The magnetic order of the samples was first examined *in situ* by surface magneto-optical Kerr effect (SMOKE). Figure 2 gives a synopsis of the measurements carried out at room temperature with the magnetic field applied in the plane of the film. By cycling the magnetic field, it is found that the Kerr response has hysterical behavior for the thicker films. The hysteresis loops show large remanence indicating ferromagnetic ordering at room temperature for the 16- and 8-Åthick iron films. As film thickness diminishes, the size of the hysteresis loop also diminishes as shown in Figs. 2(a) and 2(b). For $d_{Fe}<8$ Å, the zero remanence indicates that the film is no longer ferromagnetic. The 6-Å-thick Fe film shows a magnetization which does not saturate even at 1 kOe, and no Kerr signal was found for the 4-Å-thick film.

EXPERIMENT

The neutron measurement were carried out at the reflectometer POSY at the Intense Pulsed Neutron

Source at Argonne National Laboratory. This polarized neutron reflectometer has been already described in the literature,[26] and only a few notions will be recalled here. A well-collimated beam of pulsed neutrons exiting from a liquid-hydrogen moderator is polarized after reflection from a magnetized Co/Ti supermirror. Neutrons of all wavelengths, in the range 2.3–14.0 Å, are impinging on the flat sample surface; and after being reflected by it, are detected by a position-sensitive detector. The neutron wavelength λ is sorted out by the time of flight from the source to the detector, which amounts to a few milliseconds. The angle between the incident beam and the sample surface, θ, is typically of the order of 1^0. The reflected neutrons arrive at the detector in a well-collimated beam at an angle of 2θ with the primary beam. Other channels of the position-sensitive detector measure the neutrons scattered by lateral dishomogeneities of the sample, such as roughness at the surface or at interfaces. The reflected intensity is normalized to the neutron flux and expressed in terms of the momentum transfer, $q=4\pi\sin\theta/\lambda$. With $dq=0.0004$ Å^{-1}, the instrument is practically a very high-resolution diffractometer.

The samples were mounted on the cold finger of a He displex refrigerator, which, in turn, was positioned between the poles of an electromagnet. This provided a magnetic field transverse to the beam and parallel to the sample's surface. The neutrons were polarized parallel or antiparallel to the magnetic field of the electromagnet. The polarization efficiency was 96%. The neutron spin was turned antiparallel to the magnetic field by activating a spin flipper[23] which was 98% efficient. The neutron polarization was switched at every neutron pulse, every $\frac{1}{30}$ s, to minimize systematic errors in the collection of parallel (+) and antiparallel (−) reflectivities.

It is worthwhile to recall a few basic notions of neutron optics. The optical potential seen by neutrons in each layer is spin dependent. For + spin neutrons, $V^+=(2\pi\hbar^2/m)(bN+cB)$, where b is the average nuclear scattering amplitude and N is the average atomic density. B is the magnetic induction in the layer, generated by an assembly of aligned atomic magnetic moments μ. $c=2.3\times10^{-10}$ Å^{-2}Oe^{-1}. For − spin neutrons, $V^-=(2\pi\hbar^2/m)(bN-cB)$. In neutron reflectivity, in contrast with the reflectivity of electromagnetic waves in the visible region, the potential (or at least its nuclear component) is easily obtained from the composition and density of the material. The independence of the potential from the wavelength means that the reflectivity is solely a function of $q=4\pi\sin\theta/\lambda$, and can be obtained equivalently by varying the angle of incidence or the neutron wavelength.

The thickness dependence of the optical potential of a medium can always be approximated by a histogram, consisting of succession of layers of constant potential and appropriate thickness. The component of the neutron momentum perpendicular to the surface, $k_0=2\pi\sin\theta/\lambda$, becomes, in the ith layer:

$$k_i^{\pm}=\sqrt{k_0^2-4\pi(b_iN_i\pm cB_i)} \tag{1}$$

and the corresponding neutron wave function, obeying the Schrödiner equation:

$$\Psi_i=A_1\exp(ik_iz)+A_2\exp(-ik_iz)\ . \tag{2}$$

The amplitudes A_1 and A_2 are determined by imposing the conservation of matter and flux at each interface. At the surface $A_1=1$ and $A_2=r$, the reflectance, from which to derive the observable reflectivity $R=|r^2|$. For a general layered profile, recurrent relations[27,28] permit the exact calculation of the reflectivity.

To illustrate the effect on the reflectivity of a thin layer of iron we will use a simplified model system and approximate expressions. Suppose that the substrate has a scattering length density b_1N_1. A thin layer of iron (thickness d_2), with scattering length density $(b_2\pm cB)N_2$, is set on the top of it. Then it is covered by an overlayer of thickness d_1 of the same scattering density as the substrate. The exact expression of the reflectivity is still cumbersome; to simplify it we impose the following constraints. Since d_2 is small, we assume that $k_2d_2\ll1$. We also assume that the reflectances at all interfaces are small compared to unity ($r_{01},r_{12}\ll1$) with the same hierarchy. With these approximations, the expression we derive is valid only in a region where k_2 is nor too large, nor too close to the critical value. After some manipulations, the approximate reflectivity takes the form

$$R^{\pm}\approx R_0\left[1-4k_0d_2\frac{[(b_2N_2\pm cB)-b_1N_1]}{b_1N_1}\sin(2d_1k_1)\right]\ , \tag{3}$$

where $R_0=[(k_0-k_1)/(k_0+k_1)]^2$ is the reflectivity for an infinite slab of scattering amplitude density b_1N_1. To put explicitly the magnetic terms, we consider the polarization

$$P=\frac{R^+-R^-}{R^++R^-}\approx8k_0cBd_2\frac{\sin(2d_1k_1)}{b_1N_1}\ . \tag{4}$$

Equations (3) and (4) have an interesting form. In the first instance, if Fe was not coated ($d_1=0$) its contribution to the reflectivity would appear only in the (omitted) higher-order terms. In other words, the gold coating actually enhances the magnetic signal by introducing an oscillating term of amplitude proportional to linear magnetic flux, i.e., the product of the internal field and iron thickness (Bd_{Fe}). To the extent that $k_{Fe}d_{Fe}\ll1$, the experiment is insensitive to the variation of B within the layer, or for that matter to the thickness of the layer itself. However, the average magnetic moment per Fe can always be determined with high accuracy. This is because the scattering amplitude density of iron in Eq. (3) can be written as $(b_{Fe}\pm c'\mu_{Fe})N_{Fe}$. $c'=0.026\,95\times10^{-12}$ cm/μ_B. Even without detailed knowledge of the number of iron atoms in the layer or their density, the simultaneous fitting of R^+,R^- strongly constrains the ratio between the atomic moment and the well-known neutron scattering length of iron.

RESULTS

Figures 3 and 4 show data obtained for the 16-Å-thick sample at room temperature. Figure 3 depicts the spin-dependent reflectivity at saturation (in a magnetic field of 200 Oe) as a function of the neutron momentum transfer q. Solid dots and open circles represent, respectively, the reflectivities of neutrons with spin parallel (+) and antiparallel (−) to the applied magnetic field—and to the magnetization. For small values of q, the reflectivity is total. At the right of this region, the oscillations seen in both curves are due to the interference between waves reflected from the gold surface and the Au/Fe interface. For clarity the experimental error bars were omitted. They are instead indicated in Fig. 4 which shows the polarization $P=(R^+-R^-)/(R^++R^-)$. The polarization gives the most immediate signature of the magnetic character of the sample, being identically zero if the sample was nonmagnetic.

To calculate the reflectivity on the basis of a model profile, several parameters are needed. These are the thickness of the gold layer d_{Au}; the gold scattering amplitude density, which in the bulk is 4.5×10^{-6} Å^{-2}; the thickness of Fe; its nuclear scattering amplitude (8.00×10^{-6} Å^{-2} for bcc iron); and the corresponding magnetic amplitude (4.99×10^{-6} Å^{-2} at low temperature in the bulk). For the MgO substrate, the scattering amplitude density is 5.95×10^{-6} Å^{-2}. This value is immediately confirmed in the experiment because it gives an excellent fitting to the critical value of q at which the reflectivity becomes total. The scattering amplitude of gold was also assumed known; all the other parameters were left floating for best fitting to the data. In all cases, the exact recurrent relations were used to calculate the reflectivity. The continuous and dotted lines are the best fits obtained for the reflectivities for the two spin states.

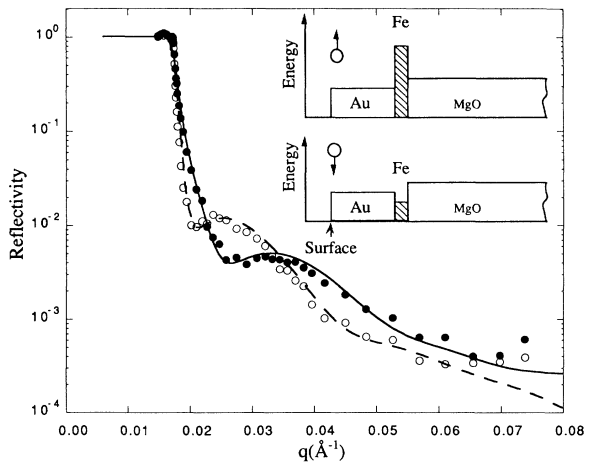

FIG. 3. Spin-dependent reflectivity of a 16 Å-thick Fe film. The data were obtained at room temperature in a magnetic field of 200 Oe. Solid dots indicate data for neutron spin parallel to the applied field (+); open circles are for spin antiparallel to the field (−). The inset is the schematic diagram of the neutron potential for + and − spin neutrons through the sample.

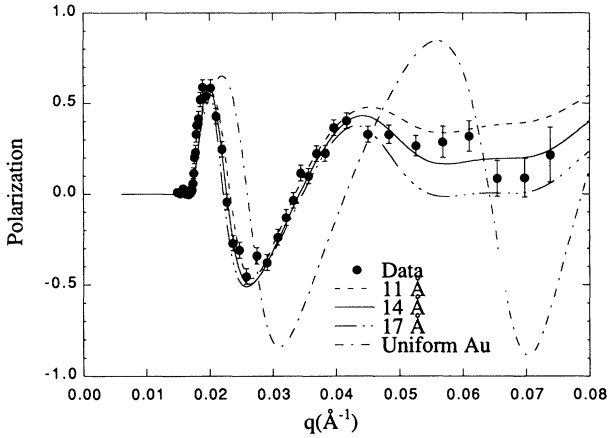

FIG. 4. Polarization function of the 16-Å sample, compared with the polarization calculated for different Fe layer thicknesses. Polarization of the uniform gold layer of 150 Å is also plotted in the figure.

$\chi^2=11$. It is worthwhile to discuss the values of the fitting parameters, their meaning, and the procedure by which they were derived.

Since the oscillation period is very sensitive to the gold thickness, special care was exercised both in conducting the experiment and in fitting the model. As mentioned above, the samples had a wedge-shaped gold coating. In the experiment the wedge was kept parallel to the neutron beam: since the sample is illuminated over its entire height the measured reflectivity is an average of the reflectivities for all component gold thicknesses. We were unable to fit the data using a model of uniform gold coverage; the fit in Figs. 3 and 4 was obtained by averaging reflectivity patterns for gold-layer thicknesses ranging from 150 to 240 Å. The main effect of averaging the reflectivities was to progressively smear out the oscillations when q is increased. However, the innermost polarization maximum remains virtually unchanged (see Fig. 4) and provides an unbiased value of the iron magnetization.

The fitted iron scattering density and the internal magnetic field B are 7.0×10^{-6} Å^{-2} and 4.0×10^{-6} Å^{-2}, respectively, and $d_{Fe}=14$ Å. These results, taken at face value, indicate that the density of Fe in the film is lower (by 13%) than the bulk Fe. In part this conclusion might be rationalized with the argument that the Fe lattice is slightly stretched to match the MgO lattice ($\Delta a\approx4\%$). Alternatively, we might try to change d_{Fe}. In the first approximation [Eq. (3)], the reflectivity depends only on the product $N_{Fe}d_{Fe}$; differences due only to higher-order terms are more readily observable in this sample with the thickest iron layer. Figure 4 shows the polarization calculated for thickness of 11 and 17 Å: the fit is worse ($\Delta\chi^2=2$) in comparison to best-fitted value. Independently from these considerations, the ferromagnetic moment per iron is determined from the ratio of the magnetic versus nuclear amplitude and it is $2.0\mu_B$. After this careful study of the "16 Å" sample, all the best-fitted values of the parameters were kept constant when fitting the reflectivity of all other samples, with the exception of d_{Fe}

and B. Actually the iron thickness was scaled down according to the thickness monitor measurements, and the only fitted parameter was the magnetization.

A synopsis of the polarized neutron reflectivity measurements is presented in Table I. At room temperature, the 8-Å film displayed a large ordered magnetic moment per iron ($2.0\mu_B$), while only a very small moment ($<0.5\mu_B$) was found in the 6-Å thick film and the 4-Å film was nonmagnetic. This is consistent with the SMOKE measurements taken at room temperature. The polarized neutron reflection measurements were then repeated at low temperature. Figure 5 shows the polarization of the 4-, 6-, and 8-Å samples at 40 K in a magnetic field of 5 kOe. As it can be seen, the magnetic signal has the identical shape for the three samples and it is only scaled according to the iron thickness. Thus, even a visual inspection of Fig. 5 strongly suggest that the iron moment remains the same for all samples. To be more quantitative, we computed reflectivity and polarization for different iron moments, to fit the experimental points (solid lines in Fig. 5). We found a magnetic moment of $2.2\pm0.2\mu_B$ for all four samples, essentially the same value of bulk iron in the bcc phase.

A number of tests was made to assure that the measurements were made for values of magnetic field and temperature such that the magnetization should be close to that of the ground state. The polarized neutron reflevity of the 4-Å film was measured at 40 K at different magnetic field and the net ferromagnetic moments per Fe were extracted and plotted in Fig. 6. Unlike for the thick films, an external field of ~ 3 kOe is needed to saturate the magnetization. The simplest explanation is that for thin films of iron the easy axis is out of plane, and a relatively large magnetic field is required to align the moments in plane. Subsequent Kerr effect measurement were performed in a separate experiment[29] on similar samples at low temperature. The measurements, carried out in the longitudinal as well as the polar geometry, also

TABLE I. Compendium of the polarized neutron measurements on Fe/MgO samples.

Fe thickness (Å)	Magnetic field (Oe)	Temperature (K)	Magnetic moment/Fe
4	200	300	0.0
6	200	300	<0.5
8	200	300	2.0±0.2
16	200	300	2.0±0.2
4	5000	90	1.7±0.2
4	200	40	0.7±0.1
4	2000	40	1.7±0.2
4	3000	40	1.9±0.3
4	4000	40	2.2±0.3
4	6000	40	2.3±0.3
4	8000	40	2.0±0.2
4	5000	40	2.2±0.2
6	5000	40	2.2±0.2
8	5000	40	2.2±0.2

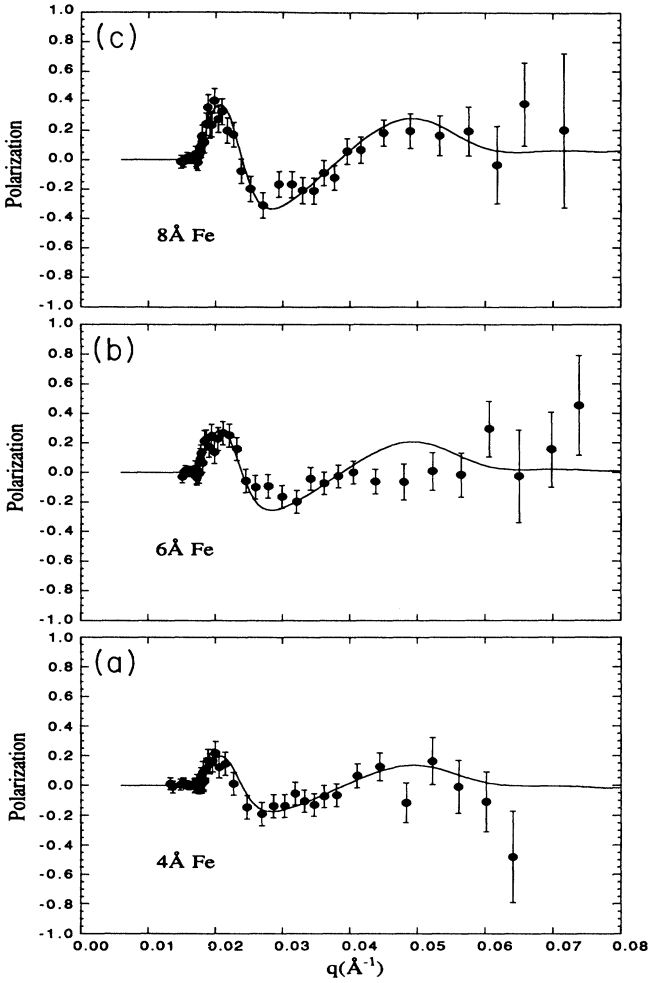

FIG. 5. Polarization functions for (a) 4-Å, (b) 6-Å, and (c) 8-Å Fe films at $T=40$ K and $H=5$ kOe. All fits used the same parameters except for the iron thickness.

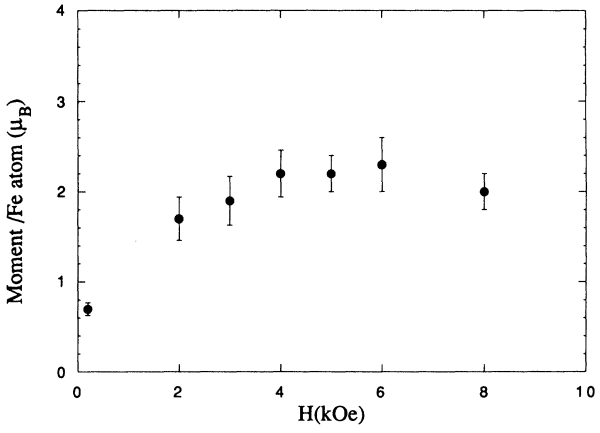

FIG. 6. Net magnetic moment of iron of the 4-Å film at 40 K, as a function of the applied field. The film could only be saturated with a magnetic field of 3 kOe, suggesting that the magnetization axis is out of plane.

suggest that the spontaneous magnetization is tilted out of the plane. Less complete was the determination of the Curie temperature. At 90 K the 4-Å film had a magnetic moment of 1.7 μ_B/Fe, to be compared with the value of 2.2 μ_B/Fe found at 40 K. It is generally accepted that T_c decreases dramatically for monolayer iron films due to the reduced dimensionality, as indeed has been shown for several systems.[30] We believe that the slight decrease in magnetic moment at 90 K for the 4-Å film is due to the decreased T_c and the magnetization at zero temperature should not be significantly different from that obtained at 40 K.

DISCUSSION

Our main result is that the magnetic moments of iron in thin films epitaxial on MgO remain equal to those of the solid regardless of the film thickness. Such a finding is in contradiction with the predicted enhancement of the iron moment in very thin films; and the question is if the experimental results are flawed by some imperfection in the samples. There is considerable evidence that the samples do not have the ideal planar geometry. As mentioned earlier, the Auger signal during growth was not exactly that typical of a layer-by-layer deposition. Also, in the course of the neutron reflectivity measurements a substantial amount of diffuse scattering was noticed, which signifies irregularities at or close to the MgO surface. However, these imperfections are unlikely to reconcile the discrepancy.

Figure 7 shows contour plots of the intensities of the neutrons scattered and reflected from the 16- and the 4-Å samples. A consistent (but somewhat surprising) trend for all samples is that the thinner the iron layer is, the stronger scattering is. For each sample, however, the scattered radiation is the same for both neutron spin states; and no correlation with temperature or magnetic field is found. The presence of scattering indicates that some interfaces are "rough," or more explicitly, that the interfaces are perfect over a distance shorter than the coherence length of the neutrons. The scattering is characterized by a ridge,[31] in with the angles of incidence θ_1 and scattering θ_2 are coupled by the equation:

$$\tfrac{1}{2}(\theta_1+\theta_2)\sqrt{\pi/bN}=\lambda\ . \tag{5}$$

In this case bN is approximately the scattering amplitude density of MgO. This pinpoints the origin of scattering to the polished, but cleavable, (100) MgO surface, as was confirmed by subsequent experiments on bare MgO substrates.

The mean height of the roughness is determined to be 6±6 Å by fitting the data using Gaussian-distributed height deviations from a perfectly flat interface. The Gaussian fluctuation gives an exponential term in reflectance and slightly depresses reflectivity[32] at large q. Still, such roughness could, in principle, have a deep effect on the magnetism of an iron layer of comparable height. Fortunately, the limited width of the diffuse scattering indicates that the fluctuations due to roughness take place over long distances. If we ideally divide the face of MgO in a number of perfect regions separated by steps, we estimate that their mean size is no less than

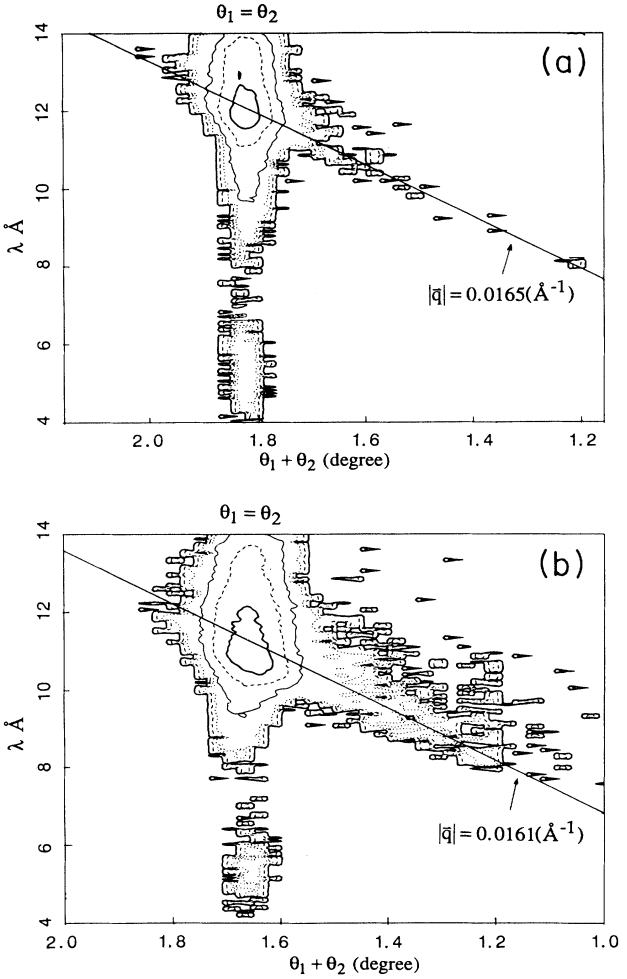

FIG. 7. Diffuse neutron scattering for (a) the 16-Å sample and (b) the 4-Å sample. The reflected beam is emitted at a fixed $2\theta_1 = 1.832°$ and 1.672° for the 16- and 4-Å samples, respectively. The scattered intensity is centered on the straight line indicated in the figure.

1000 Å. The built-in sensitivity of neutron reflectivity to even small perturbations from planar symmetry provides an added assurance of the physical validity of the results obtained.

To conclude, we note that our experimental samples are short of being perfect, but the imperfections are not sufficient to alter significantly our main conclusions: thin films of iron on MgO are ferromagnetic, with a magnetic moment practically identical to that of the solid.

ACKNOWLEDGMENTS

We would like to thank A. J. Freeman for several enlightening discussions on the expected behavior of magnetization in reduced dimensionality. We also acknowledge the substantial technical help of Rick Goyette in collecting the data and operating and maintaining the equipment. This work is supported by the U. S. Department of Energy, BES-Materials Sciences, under Contract No W-31-109-ENG-38.

[1]R. E. Watson, P. Fulde, and A. Luther, in *Magnetism and Magnetic Materials, 1972 (Denver),* Proceedings of the 18th Annual Conference on Magnetism and Magnetic Materials, AIP Conf. Proc. No. **10**, edited by C. D. Graham and J. J. Rhyne (AIP, New York, 1973), p. 32, and references within.
[2]N. D. Mermin and H. Wagner, Phys. Rev. Lett. **17**, 1133 (1966).
[3]S. Ohnishi, A. J. Freeman, and M. Weinert, Phys. Rev. B **28**, 6741 (1983).
[4]C. L. Fu, A. J. Freeman, and T. Oguchi, Phys. Rev. Lett. **54**, 2700 (1985).
[5]R. Richter, J. G. Gay, and J. R. Smith, Phys. Rev. Lett. **54**, 2704 (1985).
[6]V. L. Moruzzi, P. M. Marcus, K. Schwarz, and P. Mohn, Phys. Rev. B **34**, 1784 (1986).
[7]S. Blügel, M. Weinert, and P. H. Dederichs, Phys. Rev. Lett. **60**, 1077 (1988).
[8]C. Li, A. J. Freeman, H. J. F. Jansen, and C. L. Fu, Phys. Rev. B **42**, 5433 (1990).
[9]A. J. Freeman, A. Continenza, and Chun Li, Mater. Res. Sci. Bull. **XV** (9), 27 (1990).
[10]Chun Li and A. J. Freeman, Phys. Rev. B **43**, 780 (1991).
[11]D. Pescia, M. Stampanoni, G. L. Bona, A. Vaterlaus, R. F. Willis, and F. Meier, Phys. Rev. Lett. **58**, 2126 (1987).
[12]C. Liu, E. R. Moog, and S. D. Bader, Phys. Rev. Lett. **60**, 2422 (1988).
[13]B. Heinrich, K. B. Urquhart, A. S. Arrott, J. F. Cochran, K. Myrtle, and S. T. Purcell, Phys. Rev. Lett. **59**, 1756 (1987).
[14]N. C. Koon, B. T. Jonker, F. A. Volkening, J. J. Krebs, and G. A. Prinz, Phys. Rev. Lett. **59**, 2463 (1987).
[15]M. Stampanoni, A. Vaterlaus, M. Aeschlimann, and F. Meier, Phys. Rev. Lett. **59**, 2483 (1987).
[16]W. Dürr, M. Taborelli, O. Paul, R. Germar, W. Gudat, D. Pescia, and M. Landolt, Phys. Rev. Lett. **62**, 206 (1989).
[17]C. Liu and S. D. Bader, J. Appl. Phys. **67**, 5758 (1990).
[18]H. J. Elmers, G. Liu, and U. Gradmann, Phys. Rev. Lett. **63**, 566 (1989).
[19]T. Urano and T. Kanaji, J. Phys. Soc. Jpn. **57**, 3043 (1988).
[20]G. P. Felcher, K. E. Gray, R. T. Kampwirth, and M. B. Brodsky, Physica B **136**, 59 (1986).
[21]J. A. C. Bland, D. Pescia, and R. F. Willis, Phys. Rev. Lett. **58**, 1244 (1987).
[22]T. Kanaji, K. Asano, and S. Nagata, Vacuum **23**, 55 (1973).
[23]C. Argile and G. E. Rhead, Surf. Sci. Rep. **10**, 277 (1989).
[24]C. Egawa, T. Aruga, and Y. Iwasawa, Surf. Sci. **185**, L506 (1987).
[25]C. Liu and S. D. Bader, Phys. Rev. B **41**, 553 (1990).
[26]G. P. Felcher, R. O. Hilleke, R. K. Crawford, J. Haumann, R. Kleb, and G. Ostrowski, Rev. Sci. Instrum. **58**, 609 (1987).
[27]L. G. Parratt, Phys. Rev. **95**, 359 (1954).
[28]N. Born and E. Wolf, *Principles of Optics* (Pergamon, Oxford, 1975).
[29]C. Liu, Y. Park, and S. D. Bader, J. Magn. Magn. Mater. **111**, L225 (1992).
[30]C. Liu and S. D. Bader, Phys. Rev. B **44**, 2205 (1991).
[31]Y. Y. Huang, G. P. Felcher, and S. S. P. Parkin, J. Magn. Magn. Mater. **99** L31 (1991).
[32]S. K. Sinha, E. B. Sirota, S. Garoff, and H. B. Stanley, Phys. Rev. B **38**, 2297 (1984).